AIP Advances

Realization of multiband communications using different Rydberg final states

Cite as: AIP Advances **12**, 065118 (2022); https://doi.org/10.1063/5.0095780
Submitted: 03 May 2022 • Accepted: 24 May 2022 • Published Online: 21 June 2022

Yijie Du, Nan Cong, Xiaogang Wei, et al.

View Online Export Citation CrossMark

ARTICLES YOU MAY BE INTERESTED IN

Rydberg atom-based field sensing enhancement using a split-ring resonator
Applied Physics Letters **120**, 204001 (2022); https://doi.org/10.1063/5.0088532

Continuously tunable radio frequency electrometry with Rydberg atoms
Applied Physics Letters **121**, 014002 (2022); https://doi.org/10.1063/5.0086357

Enhancement of electromagnetically induced transparency based Rydberg-atom electrometry through population repumping
Applied Physics Letters **119**, 214001 (2021); https://doi.org/10.1063/5.0069195

© 2022 Author(s).

Realization of multiband communications using different Rydberg final states

Cite as: AIP Advances 12, 065118 (2022); doi: 10.1063/5.0095780
Submitted: 3 May 2022 • Accepted: 24 May 2022 •
Published Online: 21 June 2022

View Online Export Citation CrossMark

Yijie Du,[1,2] Nan Cong,[1] Xiaogang Wei,[1] Xiaonan Zhang,[1,2] Wenhao Luo,[1,2] Jun He,[1,3,a)] and Renfu Yang[1,a)]

AFFILIATIONS

[1] Beijing Academy of Quantum Information Sciences, Beijing 100193, China
[2] School of Instrument Science and Opto-Electronics Engineering, Beihang University, Beijing 100191, China
[3] State Key Laboratory of Quantum Optics and Quantum Optics Device, and Institute of Opto-Electronics, Shanxi University, Taiyuan 030006, Shanxi, China

[a)] **Authors to whom correspondence should be addressed:** hejun@sxu.edu.cn and yangrf@baqis.ac.cn

ABSTRACT

Rydberg atoms can serve as an atomic radio frequency receiver for digital and analog information transmission. In this paper, a ladder-type electromagnetically induced transparency system is prepared in a room temperature cesium atomic vapor cell. Microwave electric fields in the Ku band at a frequency of 12.52 GHz and the Ka band at a frequency of 39.80 GHz are used as two-channel communication carriers to demonstrate concurrent information transmission. Analog and digital communications are demonstrated by performing audio and pseudo-random binary sequence signal transmission, respectively. The dynamic range of the proposed system is ~50 dB, and the communication bandwidth is more than 10 MHz. The obtained results demonstrate the fundamental principles of two- or multi-band communication systems based on different Rydberg final states.

© 2022 Author(s). All article content, except where otherwise noted, is licensed under a Creative Commons Attribution (CC BY) license (http://creativecommons.org/licenses/by/4.0/). https://doi.org/10.1063/5.0095780

I. INTRODUCTION

Rydberg atoms have wide applications, particularly in quantum information processing, for instance, in quantum computing,[1,2] entanglement state preparation,[3,4] quantum communication,[5,6] and entanglement concentration[7] due to the properties of the interaction between Rydberg atoms and photons. Atom-based standards have been demonstrated for high-precision measurements of fundamental physical quantities, including time, length, mass, and gravitational field.[8] Electric fields (E-fields), particularly radio frequency (RF) or microwave (MW) fields, can be measured using atom-based electricity via quantum interference effects, i.e., using electromagnetically induced transparency (EIT) and Autler–Townes (AT) splitting with Rydberg atoms over a wide range from sub-MHz to THz frequencies in room temperature vapor cells.[9–12]

Atom-based sensors and antennas are expected to enable further unique capabilities for sensing and communication applications.[12,13] This emerging quantum technology has demonstrated several significant advantages, including high sensitivity, intrinsic accuracy, compact system size, and broad tunability. Rydberg atoms with a principal quantum number $n \gg 1$ have large electric dipole transition moment ($\sim n^2$) and polarizability ($\sim n^7$) values.[14] Rydberg atom-based MW E-field measurements are superior to those of conventional antenna-based techniques because they enable self-calibrated electric field measurements to be traceable directly to Planck's constant. Since the seminal work done by Sedlacek *et al.* in 2012, in which they realized a sensitivity of $\sim 30\ \mu\text{V/cm}/\sqrt{\text{Hz}}$ in rubidium (Rb) Rydberg atom-based electrometry, intensive research efforts have been made in the MW electrometry field.[15] Due to the photon shot noise, the sensitivity of atom-based electrometers is $\sim 2\ \mu\text{V/cm}/\sqrt{\text{Hz}}$ at best.[16] By using atomic superheterodyne technology, Jing *et al.* showed that the cesium (Cs) Rydberg atom-based superheterodyne receiver can achieve a sensitivity of $\sim 55\ \text{nV/cm}/\sqrt{\text{Hz}}$.[17] These results indicate that increased sensitivity can be expected in Rydberg atom-based electrometry.

Recently, Rydberg atom-based antennas for MW E-field applications have also been investigated for use in wireless communication. Communication technologies are having an increasing impact on economic activity, scientific research, and national defense demands. The MW technology is the foundation of modern

© Author(s) 2022

communications and has many other applications, including several in health and medical science technologies. A Rydberg atom EIT-based approach has been demonstrated to realize both digital and analog communications using an amplitude modulation (AM) approach.[2,18–21] Specifically, a proof-of-principle work for multi-channel communications that uses the same pair of Rydberg states with certain RF detuning has been presented.[18] Eight-state phase-shift-keying digital communication was also realized using Rb Rydberg atoms.[19] For analog signal transmission, ensembles of atoms comprising Cs and Rb atoms have been used to achieve musical recording and AM-based broadcasting.[21] Moreover, by dressing pairs of Rydberg states, Deb and Kjærgaard encoded RF signals in the light via "radio-over-fiber" and they have demonstrated a bandwidth over 1 MHz.[2]

In this work, we perform the AM of the MW baseband carriers and detect the EIT signal. We then demonstrate the realization of concurrent two-channel analog and digital communications based on Cs Rydberg atoms using two different separated states, i.e., $66S_{1/2} \leftrightarrow 66P_{1/2}$ (12.5 GHz) and $66S_{1/2} \leftrightarrow 67P_{3/2}$ (39.8 GHz). Specifically, two-channel audio transmission has been demonstrated successfully in our Rydberg atom-based system at room temperature. MW communication has also been demonstrated by transmitting a pseudo-random binary sequence (PRBS) signal through one channel and two individual carrier channels.

II. EXPERIMENTAL SETUP

Figure 1 shows a diagram of the experimental setup. An 852 nm laser beam from an external cavity diode laser (ECDL) with a typical linewidth of ~100 kHz was used as a probe laser. The output optical power from a 1018 nm ECDL laser was amplified up to 5 W using an ytterbium-doped fiber amplifier (YDFA) and was then frequency-doubled using a periodically poled lithium niobate (PPLN) crystal to produce a 509 nm laser beam. The size of the probe beam was 350 μm, and the size of the coupling laser beam was 480 μm. These two beams were then overlapped in a cesium atomic vapor cell using a counterpropagating configuration. The 852 nm ECDL was locked to the D_2 transition of $6S_{1/2}$ (F = 4) → $6P_{3/2}$ (F = 5) via saturation absorption spectroscopy (SAS) of Cs. The 509 nm fiber laser was stabilized through EIT spectroscopy using the servo system highlighted in Fig. 1. The RF signal generator (Rohde & Schwarz, SMA100B) was stabilized by connecting it to a Rb atomic clock (Stanford Research Systems, FS725). The photoelectric signal was obtained using either an oscilloscope (Keysight, DSOX3024T) or a spectrum analyzer (Keysight, 9030B).

III. EXPERIMENTAL RESULTS AND DISCUSSION

Figure 2(a) shows the atomic energy level scheme used for these experiments. The 852 nm probe laser and the 509 nm coupling laser were nearly resonant. The EIT transmission signal was monitored by scanning the coupling laser frequency while locking the probe laser frequency to avoid the Doppler background in the spectra. The strong coupling laser was scanned across the upper transition. The EIT peak appeared when the probe laser and the coupling laser were two-photon resonant, as shown by the black line in Fig. 2(b). Using an RF modulation technique, we measured the full width at half maximum (FWHM) of the EIT spectrum to be ~5 MHz. An MW E-field at a frequency of 12.5 GHz, which is resonant with two adjacent Rydberg levels ($66S_{1/2} \leftrightarrow 66P_{1/2}$), caused the EIT signal to decrease or to split via the AT effect.

Figure 2(b) shows the probe signal spectra obtained with different MW E-field powers. When the MW E-field increases, the peak of the EIT signal decreases and its FWHM broadens as a result of power broadening (see the red line). When the MW E-field power continues to increase, the main EIT peak then splits into two peaks (see the blue and magenta lines). Furthermore, this split becomes wider as the MW power increases continuously, as illustrated by the

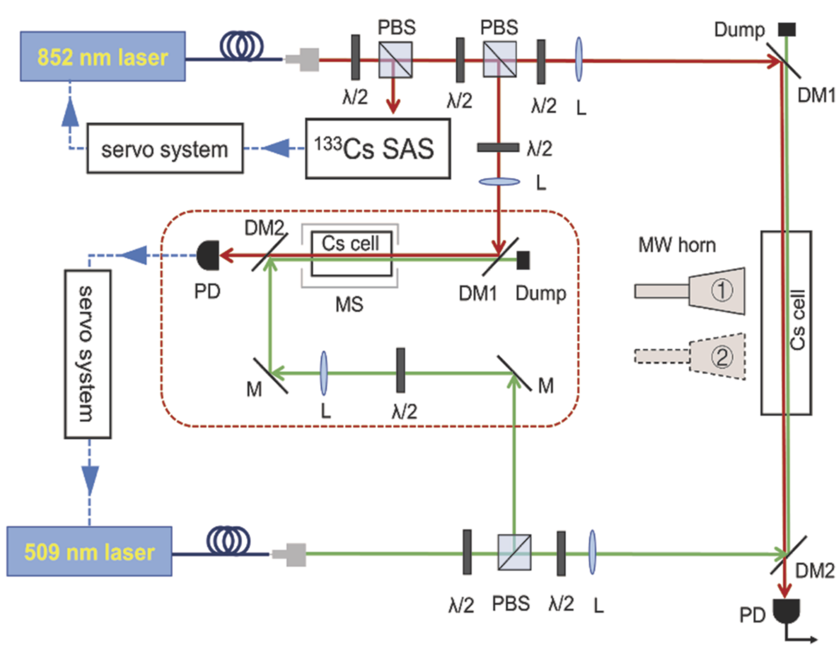

FIG. 1. Experimental apparatus used for MW E-field measurements and MW communications. The 852 nm ECDL was used as a probe laser. The 509 nm laser was used as a coupling laser. The 852 and 509 nm laser beams were then overlapped in the Cs cell using a counterpropagating configuration. Two MW horns were used in our experiments. The first horn is marked ①, and the second is marked ②. The first horn provided a signal output of 12.5 GHz. The second horn provided the 39.8 GHz carrier in the two-channel communication demonstration. λ/2: half-wave plate, PBS: polarizing beam splitter cube, L: lens, MS: magnetic shielding, PD: photodiode detector, M: mirror, DM1: 852 nm high reflectivity (HR) and 509 nm high transmissivity (HT) dichroic mirror, DM2: 852 nm HT and 509 nm HR dichroic mirror, and SAS: saturation absorption spectroscopy.

© Author(s) 2022

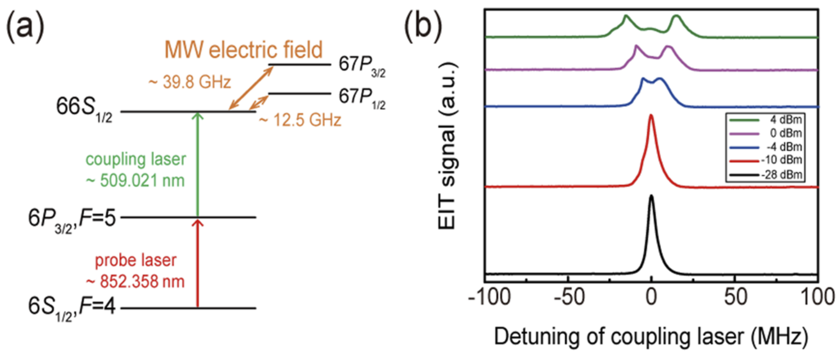

FIG. 2. (a) Illustration of typical ladder-type EIT of cesium atoms with 12.5 and 39.8 GHz microwave transitions. (b) EIT-AT splitting behavior for 12.5 GHz under different microwave E-field power level.

olive line in Fig. 2(b). The shape of EIT-AT spectra distorted at high level RF transmitted strength. This is mainly due to the inhomogeneous distribution of the space RF field over the vapor cell and the vector character of the RF field. A high strength RF field will reflect when it encounters the metal surface, e.g., optical platform and mirror frame, resulting in the inhomogeneous distribution of the RF around the Rydberg atom vapor cell. The effect resulted from the positioning of the antenna that was required to avoid unwanted reflections. The slight asymmetry in the data is due to a small amount of ionization.[22,23] By measuring the width of this split, the MW E-field strength can be obtained using the formula $|E| = 2\pi\Delta f_0\hbar/\mu$, where $\hbar$ is the reduced Planck constant, μ is the atomic electric dipole moment of the MW transition, and Δf_0 is the measured EIT split. When the MW E-field is not strong enough to cause the splitting for EIT, the maximum probe transmission signal will then decrease as a function of the MW E-field.

The MW E-field can also be determined via the modified transmission of the EIT signal, where the smooth decay signal can be used to perform the communication function. The dynamic MW E-field power and frequency ranges of our system were also evaluated. The system can achieve a nearly linear dynamic range of over 50 dB for MW E-fields, and the frequency response was ~100 MHz when the MW E-field power was −40 dBm (Figs. S1 and S2 in the supplementary material). This means that digital communication using continuously tunable MW carriers in an off-resonance scheme is feasible. Based on the transmission of the EIT signal and the use of AM technology, we obtained a minimum E-field power of ~−70 dBm.

The Rydberg atom antenna can act as a receiver to detect and receive MW E-field signals. We, therefore, demonstrated the conversion of MW signals into optical signals and performed a demonstration based on audio frequency and PRBS signals. In this approach, a continuous wave carrier was amplitude-modulated using an audio source from a computer. The PRBS signals were generated using an arbitrary waveform generator (Keysight, 335 00B) and encoded to the MW carrier via external AM. The audio frequency carrier signal and the PRBS signal were then received by the Rydberg atom and transformed into an intensity signal of the probe laser beam, which was detected using a photodetector (PD). A lock-in amplifier (Zurich Instruments, MFLI) was used to demodulate the audio signal or the PRBS signal from the MW carriers.

The optimum communication rate of 10 Mbps is bounded by the EIT bandwidth, which is mainly limited to the Rabi frequency of the coupling laser in this case. The EIT bandwidth is limited to the time needed to excite the atoms to the Rydberg state. The bandwidth evaluation can be inferred from the signal-to-noise ratio (SNR) of the AM technique. Figure 3 shows the SNR corresponding to the AM modulation frequency with 12.52 GHz microwave transition. In the current experimental system, modulation frequencies from 7 to 300 kHz provide an optimum SNR of more than 50 dB. It is important to note that many factors could affect the SNR of the system, including the coupling laser power, atomic density, and technical noise from the photodiode detector, just to mention a few. A response bandwidth of 10 MHz to an incident time-variant MW E-field can be achieved for the Rydberg antenna in our system, in which the SNR is greater than 10 dB.

The Rydberg atom EIT-based sensor can act as a highly sensitive atomic receiver to enable communication applications. However, two-channel or multiple-channel information transmission can be challenging. Here, we have demonstrated two-channel communication implemented using two Rydberg final states, $66S_{1/2} \leftrightarrow 66P_{1/2}$ (12.5 GHz) and $66S_{1/2} \leftrightarrow 67P_{3/2}$ (39.8 GHz). The results of our study of the coupling behavior of the two channels are shown in Fig. 4. In the experiment, one channel was in the Ku band, with the

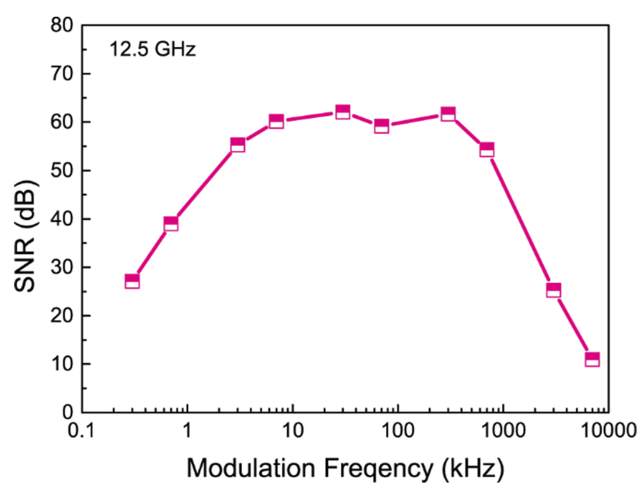

FIG. 3. The signal-to-noise ratio (SNR) corresponds to the AM modulation frequency with 12.52 GHz microwave transition. The SNR is larger than 10 dB with a maximum modulation frequency of 10 MHz.

© Author(s) 2022

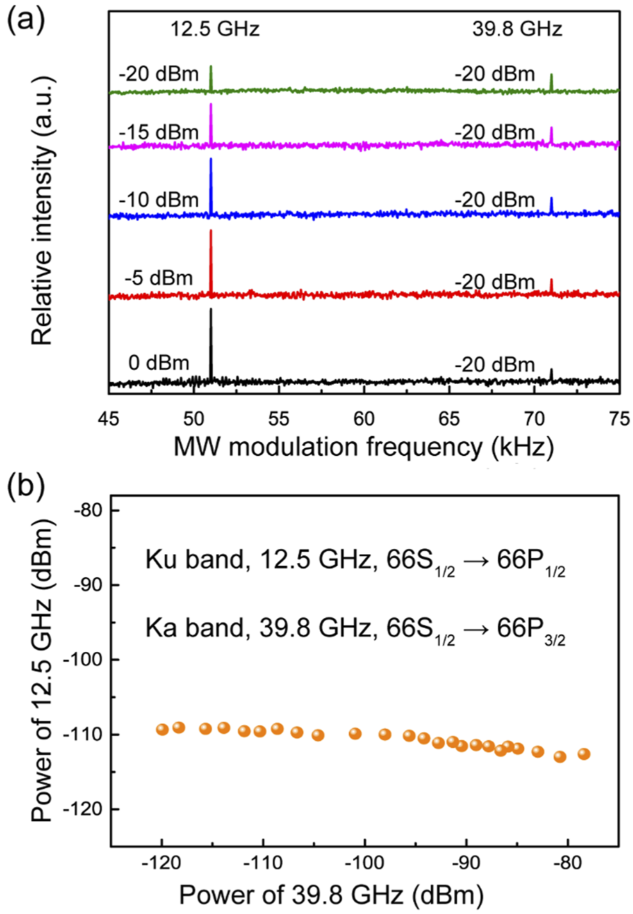

FIG. 4. Interactions between the 12.5 and 39.8 GHz microwave carriers: (a) 12.5 GHz carrier microwave power variation from −20 to 0 dBm with the 39.8 GHz carrier microwave power remaining fixed at −20 dBm and (b) 12.5 GHz carrier microwave power variation when the 39.8 GHz carrier microwave power changed from −120 to −78 dBm.

12.5 GHz ($66S_{1/2} \leftrightarrow 66P_{1/2}$) signal modulated by a 51 kHz sinusoidal wave internally using an RF signal generator. The other channel was in the Ka band, with the 39.8 GHz ($66S_{1/2} \leftrightarrow 67P_{3/2}$) signal modulated by a 71 kHz sinusoidal wave. These two MW E-field carriers were sent simultaneously to the Cs vapor cell using two MW horns, as illustrated in Fig. 1. The detected probe laser signal was demodulated using the lock-in amplifier and analyzed using a spectrum analyzer. In Fig. 4(a), the 39.8 GHz channel maintains its transmission level at −20 dBm, while the level of the 12.5 GHz channel is tuned from −20 to 0 dBm. Figure 4(b) shows the clear crosstalk-free behavior of the 12.5 GHz MW carrier when the 39.8 GHz transmission level changes from −120 to −78 dBm. Both results show that these two channels can be demodulated independently from each other.

Audio signals (music recordings) were added to the MW carriers by external AM. The same audio signals were added to the two carriers. Before loading the audio to the microwave, we stabilized the frequency of lasers by using the reference EIT spectrum. This means that the system of 852 and 509 nm lasers is two-photon resonant. The EIT signal is detected using a photodetector and then monitored using an oscilloscope. Figure S3 in the supplementary material depicts the schematic diagram of the audio modulation. The microwave signal of 12.52 GHz is modulated with a frequency of 51 kHz, and a signal of 39.80 GHz is modulated with a frequency of 71 kHz. The RF signal generator produced the AM-modulation function. The audio signal is loaded to the modulated frequencies externally via the signal generator. The modulated RF signals can be written as $S_m(t) = [k_a \exp(i\omega_a t) \times k_m \exp(i\omega_m t)] \times \exp(i\omega_{RF} t)$, where k_a and k_m represent the modulation depths, ω_a denotes the audio frequency, ω_m denotes the modulation frequency, and ω_{RF} denotes the RF carrier frequency. The modulated RF signals are radiated to the vapor cell via two horns. Rydberg atoms receive the microwave and transform the intensity signal of the probe laser to voltage via the photodetector. The voltage is demodulated by the lock-in amplifier. The residuals between the demodulated and original audio signals, $|S_{dem}(t) - S_o(t)|$, are determined to show the qualification of the demodulations.

Figure 5 records a 100 s period of original (black) and two demodulation musical waveforms (red and blue). The gray lines in the demodulation reflect the residuals. The details of the audio signal are recovered well in both demodulated signals. Furthermore, the two demodulated music wave signals were input into electric speakers. In practical, after broadcasting from the speaker, the demodulation signals have a small amount of noise compared to the original music, but they have a very minor effect on the quality of the sound. This real-time two-channel audio transmission of the same signal increases the audio signal above the noise, and this approach therefore enables high-fidelity audio transmission. The ability of the Rydberg atom EIT-based system to sense the musical composition is thus demonstrated unambiguously. Based on these results, we have reason to believe that musical duets can also be accomplished using our proposed system.

Generally, when signals are loaded at two separate modulation frequencies with the same baseband, two-band communication

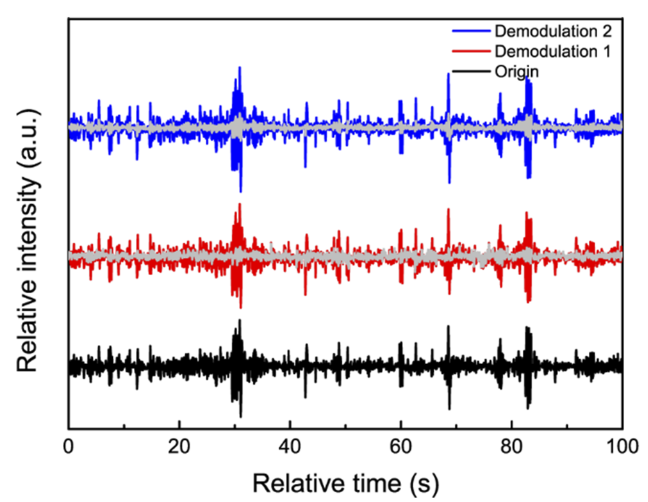

FIG. 5. Waveforms from two-channel demodulation of 100 s audio signals. The black line shows the original signal. The red and blue lines show the demodulated signals. The gray lines show the residual signal of the demodulated waveforms.

© Author(s) 2022

can be achieved by using lock-in amplifier demodulation and filter if these two modulation frequencies separate far enough. In this work, we propose a novel experimental scheme that realizes concurrent two-channel analog and digital communications based on Cs Rydberg atoms with two different separated quantum states. Herein, 51 and 71 kHz modulation frequencies (channels) are chosen, and they give decent results. It is worthy to note that the modulation frequency (channel) from 7 to 700 kHz can also give satisfactory results, as shown in Fig. 3. As each baseband is over 10 MHz, the capacity can be extended a lot via different Rydberg states.

A demonstration of digital communication was performed using PRBS signal transmission. PRBS signals are recommended by the International Telecommunication Union for digital transmission testing.[24] Figure 6 shows the waveform used for the two-channel PRBS transmission. In Fig. 6(a), the system has been shown to perform two-channel transmission of PRBS signals (transfer bit rate: 1 kbps) independently but simultaneously. The waveforms plotted in blue and magenta represent the original signals obtained from the arbitrary waveform generator. The black and red lines show the corresponding demodulated waveforms. The comparison of these demodulated waveforms with the original ones clearly shows that both the two-channel PRBS signals are transmitted with high transfer fidelity in real time. Figure 6(b) shows the results obtained when the same PRBS signal was transferred using the two-channel carrier transmission method simultaneously at a transfer bit rate of 10 kbps. The blue line shows the original waveform, and the other two lines show the demodulated waveforms. Generally, both channels can recover the original waveform, with the exception of the tiny imperfections shown in the black line. These results indicate that our system can realize digital communication and that the signal can be recognized clearly.

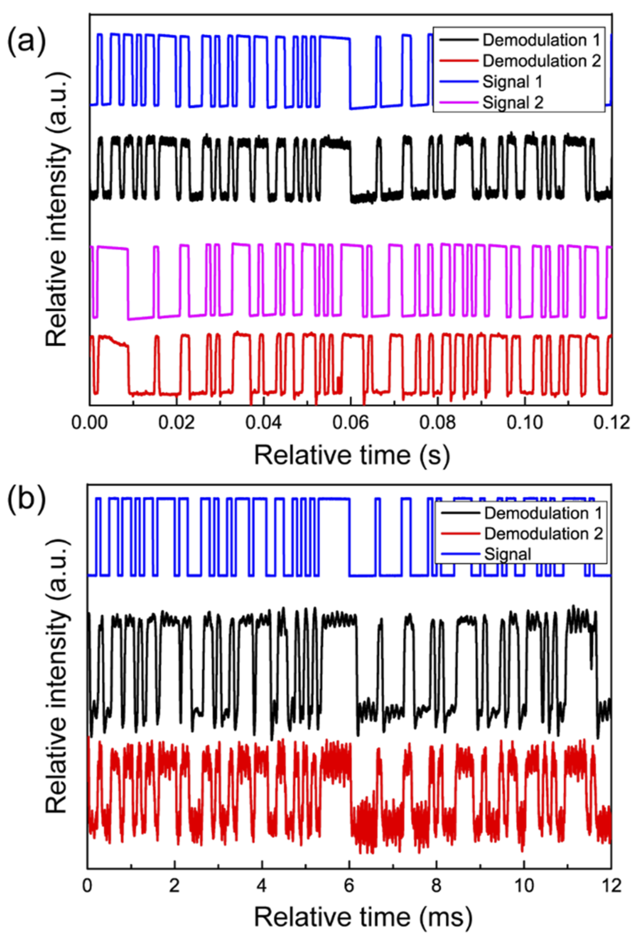

FIG. 6. Waveforms from the two-channel demodulation of the PRBS signals: (a) two-channel demodulation of two PRBS signals with a bit rate of 1 kbps and (b) two-channel demodulation of the same PRBS signals with a bit rate of 10 kbps.

The effective baseband bandwidth for this communication system is ~10 MHz, which is limited by the Rydberg atom EIT. In this case, the bandwidth is also limited by the photodetector used in our system. It is expected that a photodetector with a wider response and better linearity will contribute to a higher SNR and, thus, lead to an improved communication capability. This Rydberg atom EIT-based sensor can thus act as an antenna to enable communication applications. Multiple-channel information transmission is more challenging. Using the $66S_{1/2}$ state as the initial quantum state, we have implemented pairwise cross-communication, where the MW coupled final states include $65P_{1/2}$ (15.21 GHz), $65P_{3/2}$ (14.27 GHz), $66P_{1/2}$ (12.52 GHz), $66P_{3/2}$ (13.41 GHz), $67P_{1/2}$ (38.96 GHz), and $67P_{3/2}$ (39.80 GHz). In principle, with optimum experimental design, multiband communication can therefore be achieved. It should be emphasized here that the crosstalk will increase under strong MW transmission power conditions. In our experimental system, the MW power must be limited to less than −20 dBm for crosstalk-free communication.

So far, to realize concurrent two-band communication based on the Rydberg atoms, researchers have presented three kinds of methods. The first is based on the two species of atoms (Rb and Cs) as shown by Holloway *et al.*,[23] and in this case, different Rydberg atoms are employed to work separately and thus circumvent the crosstalk effect. This needs both atoms to work steadily. In the second method, only one species, for example, Cs, is used but with the two (or more) different coupling lasers. In this case, atoms populate at different initial Rydberg states. As long as the initial Rydberg states have enough atoms excited from the ground state $6S_{1/2}$ ($F = 4$), the concurrent multiband communication can be realized. Generally, the bandwidth of the absorption spectra of Cs is at the scale of hundreds of MHz,[13] while the Rabi frequency of the probe and coupling laser is scaled as dozens of MHz and several MHz, respectively. This means that the requirements for two different initial Rydberg states for two-band communication can be always satisfied. Finally, in the third method, as shown in this work, only one initial Rydberg state is employed and coupled with different final states. In this case, the limitation is the linewidth (or the lifetime) of the Rydberg states. Theoretically, the linewidth of the Rydberg state (e.g., $66P_{1/2}$) is several kHz. Practically, however, the linewidth is scaled as MHz accounting for the temperature, power of the lasers, transit time, etc. Therefore, the requirement for MW to realize multiband communication is that the Rabi frequency of the MW carriers should be no more than the linewidth of the Rydberg states. Otherwise, a high-power level will bring about crosstalk. In our experiment, the MW power level is less than −20 dBm.

© Author(s) 2022

Communication security is high on the practical application of priorities. Crossband information communication is realized by loading information into two or more bands. Multiband information transmission means that the information is loaded on different RF bands for communication. Even if a certain RF band is disturbed, the remaining RF bands can still ensure safe communication. In the previous work, it was reported that multi-channel communication was realized by using the vapor cell containing Rb and Cs atoms. However, this method is complex and requires at least four lasers to work at the same time. In our work, single atomic species (Cs) is used to receive different signals. It realizes concurrent two-band communications based on Cs Rydberg atoms with two different separated quantum states. One is located in the Ku band, and the other is located in the Ka band. This method can improve the anti-interference ability of communication and ensure communication security.

IV. CONCLUSION

In summary, we have built a Cs Rydberg atom experimental system and demonstrated MW E-field-based sensing and communication applications. The dynamic range of our system is ~50 dB. Based on the EIT of a Rydberg atom in a room temperature Cs vapor cell, we have successfully demonstrated an approach to realize concurrent two-channel transmission of audio and PRBS signals on AM MW E-field carriers. In addition, the two-channel carriers can transfer the information in the Ku and Ka bands independently from each other because of the features of the separate Rydberg states. The MW transmit power level used is relatively strong in the experiment. This proof-of-principle demonstration, however, has much optimization room for realization of the best sensitivity in the Rydberg atom-based system. Our work shows great promise for the development of the multi-channel Rydberg atom EIT-based digital communication range from the MHz band to the THz band in future work. This system may contribute to increased safety in information communication for future applications.

SUPPLEMENTARY MATERIAL

See the supplementary material for the dynamic range, the frequency response, and a detailed description of the two-band communication scenario of the studied Rydberg atom receiver system.

ACKNOWLEDGMENTS

This work was supported by financial funding from Beijing Municipality. J.H. acknowledges the financial support from the National Natural Science Foundation of China (Grant No. 61875111).

AUTHOR DECLARATIONS

Conflict of Interest

The authors declare that they have no conflicts of interest.

Author Contributions

Yijie Du: Conceptualization (equal); Investigation (lead); Writing – original draft (lead); Writing – review & editing (lead). **Nan Cong:** Conceptualization (equal); Investigation (equal). **Xiaogang Wei:** Investigation (supporting); Writing – review & editing (supporting). **Xiaonan Zhang:** Investigation (supporting); Writing – review & editing (supporting). **Wenhao Luo:** Investigation (supporting); Writing – review & editing (supporting). **Jun He:** Conceptualization (equal); Data curation (equal); Funding acquisition (equal); Investigation (equal); Supervision (equal); Writing – original draft (equal); Writing – review & editing (equal). **Renfu Yang:** Conceptualization (equal); Funding acquisition (lead); Supervision (lead); Writing – review & editing (equal).

DATA AVAILABILITY

The data that support the findings of this study are available from the corresponding authors upon reasonable request.

REFERENCES

[1] X.-F. Shi, Front. Phys. **16**(5), 52501 (2021).
[2] A. B. Deb and N. Kjærgaard, Appl. Phys. Lett. **112**(21), 211106 (2018).
[3] D. X. Li, C. Yang, and X. Q. Shao, Quantum Eng. **3**(2), e66 (2021).
[4] C. Yang, D. Li, and X. Shao, Sci. China: Phys., Mech. Astron. **62**(11), 110312 (2019).
[5] Y.-F. Yan, L. Zhou, W. Zhong, and Y.-B. Sheng, Front. Phys. **16**(1), 11501 (2021).
[6] L. Yang, J. Wu, Z. Lin, L. Yin, and G. Long, Sci. China: Phys., Mech. Astron. **63**(11), 110311 (2020).
[7] L. Zhou, J. Liu, Z. K. Liu, W. Zhong, and Y. B. Sheng, Quantum Eng. **3**(2), e63 (2021).
[8] T. C. Liebisch, J. Stenger, and J. Ullrich, Ann. Phys. **531**(5), 1800339 (2019).
[9] Y. Jiao, L. Hao, X. Han, S. Bai, G. Raithel, J. Zhao, and S. Jia, Phys. Rev. Appl. **8**(1), 014028 (2017).
[10] S. A. Miller, D. A. Anderson, and G. Raithel, New J. Phys. **18**(5), 053017 (2016).
[11] H. Fan, S. Kumar, J. Sheng, J. P. Shaffer, C. L. Holloway, and J. A. Gordon, Phys. Rev. Appl. **4**(4), 044015 (2015).
[12] D. H. Meyer, Z. A. Castillo, K. C. Cox, and P. D. Kunz, J. Phys. B: At., Mol. Opt. Phys. **53**(3), 034001 (2020).
[13] C. T. Fancher, D. R. Scherer, M. C. S. John, and B. L. S. Marlow, IEEE Trans. Quantum Eng. **2**, 3501313 (2021).
[14] T. F. Gallagher, *Rydberg Atoms* (Cambridge University Press, 2005).
[15] J. A. Sedlacek, A. Schwettmann, H. Kübler, R. Löw, T. Pfau, and J. P. Shaffer, Nat. Phys. **8**(11), 819–824 (2012).
[16] S. Kumar, H. Fan, H. Kübler, A. J. Jahangiri, and J. P. Shaffer, Opt. Express **25**(8), 8625–8637 (2017).
[17] M. Jing, Y. Hu, J. Ma, H. Zhang, L. Zhang, L. Xiao, and S. Jia, Nat. Phys. **16**(9), 911–915 (2020).
[18] Z. Song, H. Liu, X. Liu, W. Zhang, H. Zou, J. Zhang, and J. Qu, Opt. Express **27**(6), 8848–8857 (2019).
[19] D. H. Meyer, K. C. Cox, F. K. Fatemi, and P. D. Kunz, Appl. Phys. Lett. **112**(21), 211108 (2018).
[20] Y. Jiao, X. Han, J. Fan, G. Raithel, J. Zhao, and S. Jia, Appl. Phys. Express **12**(12), 126002 (2019).
[21] C. L. Holloway, M. T. Simons, A. H. Haddab, C. J. Williams, and M. W. Holloway, AIP Adv. **9**(6), 065110 (2019).
[22] J. A. Sedlacek, A. Schwettmann, H. Kubler, and J. P. Shaffer, Phys. Rev. Lett. **111**(6), 063001 (2013).
[23] C. L. Holloway, J. A. Gordon, S. Jefferts, A. Schwarzkopf, D. A. Anderson, S. A. Miller, N. Thaicharoen, and G. Raithel, IEEE Trans. Antennas Propag. **62**(12), 6169–6182 (2014).
[24] P. H. Bardell, W. H. McAnney, and J. Savir, *Built-In Test for VLSI: Pseudorandom Techniques* (Wiley-Interscience, 1987).

© Author(s) 2022